energies

MDPI

Article

Research on Vibration Characteristics of an Underground Powerhouse of Large Pumped-Storage Power Station

Lijuan Zhang [1], Yaohua Guo [2,3,*], Haijun Wang [2,3], Xuliang Yang [1] and Jijian Lian [2,3,4]

[1] School of Civil and Transportation Engineering, Qinghai Minzu University, Qinghai 810007, China
[2] State Key Laboratory of Hydraulic Engineering Simulation and Safety, Tianjin University, Tianjin 300072, China
[3] School of Civil Engineering, Tianjin University, Tianjin 300072, China
[4] Marine Energy and Intelligent Construction Research Institute, Tianjin University of Technology, Tianjin 300072, China
* Correspondence: guoyaohua@tju.edu.cn

Abstract: With the rapid development of pumped storage, the vibration problems caused by the operation of power stations have become increasingly prominent. In this paper, a large-scale pumped-storage power station is taken as the research object, and a three-dimensional refined finite element model of the underground powerhouse including the surrounding rock mass is established. Based on the analysis of the vibration source of the powerhouse and the water diversion pipeline, the modal and dynamic response analysis of the underground powerhouse of the hydropower station is carried out, and the distribution law of the larger vibration displacement position is revealed. The calculation results show that under the premise that the vibration source is selected reasonably and the numerical model is accurate, the main frequency of the underground powerhouse structure can be obtained more accurately. After optimizing the design of the underground powerhouse based on the calculation results, the resonance problem of the underground powerhouse of the hydropower station can be avoided. The dynamic elastic modulus of the rock mass around the underground powerhouse has little influence on the mode shape of the powerhouse, but has a great influence on its fundamental frequency. When the dynamic elastic modulus of the rock mass increases by 50%, the fundamental frequency of the plant increases by about 29%. At the same time, the mode shape of each order of the underground powerhouse structure does not change much, mainly manifested as the vibration of the beam system structure, which is mainly caused by the stiffness of the beam system components being much smaller than the structural stiffness of the windshield, machine pier, and mass concrete around the volute. The research results can provide references for the design of underground powerhouses of large-scale pumped-storage power stations and the analysis of vibration problems.

Keywords: pumped storage power station; underground powerhouse; vibration; modal analysis; steady state response

Citation: Zhang, L.; Guo, Y.; Wang, H.; Yang, X.; Lian, J. Research on Vibration Characteristics of an Underground Powerhouse of Large Pumped-Storage Power Station. *Energies* **2023**, *15*, 9637. https://doi.org/10.3390/en15249637

Academic Editor: Attilio Converti

Received: 5 December 2022
Accepted: 16 December 2022
Published: 19 December 2022

1. Introduction

Because renewable energy itself has the characteristics of randomness, seasonality, and volatility, after it is integrated into the grid on a large scale, it will often cause problems, such as irregular frequency fluctuations in the grid. As a result, it increases the difficulty of peak-shaving and valley-filling and frequency modulation and phase modulation of the power grid, which affects the quality of power supply [1,2]. In this regard, it is necessary to further optimize the layout of the power system to build a more secure, economical, intelligent, efficient, and ecologically friendly power energy system. In order to avoid the above-mentioned problems in the power grid after the large-scale integration of new energy sources, it is necessary to take targeted measures in terms of increasing reserve capacity and optimizing dispatching methods [3–5]. In recent decades, the research and development of

energy-storage technology has been valued by the energy, transportation, electric power, telecommunications, and other departments of various countries. Renewable energy can be used more effectively only when combined with energy storage, and energy storage is mainly divided into two types: electricity storage and heat storage. Compared with electricity storage, heat storage has lower cost and higher efficiency, and it is also a hot research topic at present [6–8]. In addition, pumped storage is the most widely used new energy-storage system. Pumped storage plays an irreplaceable role in ensuring the safe and stable operation of the power system due to its strong peak-shaving capability, high safety factor, large-scale energy storage, and fast response [9–11].

Pumped storage is currently the most mature technology and has the best economy and the most large-scale development conditions for the power system, which is green, low-carbon, clean, and flexible, and has a good coordination effect with wind power, solar power, nuclear power, and thermal power [12–14]. The pumped-storage power station is mainly composed of upper reservoirs, water-delivery systems, underground powerhouse systems, lower reservoirs, and other buildings, which can convert low-value energy into high-value energy. When the power grid load is low, the excess electric energy is used to pump the water from the lower reservoir to the upper reservoir and store it in the form of potential energy to improve the utilization level of new energy. When the power-grid load peaks, the potential energy of the upper reservoir is converted into high-value electric energy through the water-diversion power-generation system [15,16], making room for new energy consumption.

With the rapid development of the construction of pumped-storage power stations, due to the operation characteristics of the pumped-storage power station units with high-speed, high-water head, large capacity, and frequent switching between pumping and power-generation conditions, the vibration problems of the units and workshops are higher than those of conventional power stations. The vibration response frequency is much higher than that of conventional power stations, and it is often accompanied by noise pollution [17–19]. In actual engineering, many pumped-storage power stations have problems caused by vibration, including economic loss caused by the reduction in unit efficiency, safety problems caused by severe vibration of the plant structure, and even local structural damage that affects the normal operation of the entire power station [20,21]. Plant vibration is a comprehensive response to the combined action and excitation of multiple factors, such as "structure-hydraulic-mechanical-electromagnetic" factors. Due to the characteristics of a high-speed, high-water head and frequent changes in pumping and power-generation conditions [22,23], pumped-storage power plants have more prominent vibration problems in units and workshops than in conventional power plants.

The current design codes for powerhouses of hydropower stations in various countries address the structural vibration of powerhouses, which cannot be well adapted to the actual situation of pumped-storage power stations and need to be further improved [24,25]. The existing codes have detailed regulations and specific methods on the overall structural layout of the factory building, static and dynamic analysis, stiffness check and structural bearing capacity, etc., and also stipulate the vertical dynamic displacement and vibration frequency of the relatively rigid machine pier, and dynamic loads such as mechanical eccentric force are considered. However, it does not explain that the dynamic load combination in the anti-vibration design of the pumped-storage power station needs to consider the characteristics of hydraulic vibration, frequent switching between pumping and power-generation conditions, and cross-operation of multiple units. Moreover, the vibration safety control standards for each component of the plant are not clearly stipulated. Therefore, the research on the vibration problem of pumped-storage power stations is more important than that on those of conventional hydropower stations.

2. Analysis of Vibration Source Characteristics of Underground Powerhouse

2.1. Vibration Source Analysis

The causes of vibration in the hydropower plant area are divided into electrical, mechanical, hydraulic, etc., pulsation [26,27] The mechanism of unit vibration caused by electrical and mechanical defects is that the frequency of the exciting force generated by the electrical and mechanical and the frequency of unit rotation form resonance to cause the unit to vibrate. Therefore, in the vibration theory, the vibration caused by electricity and machinery can be classified as the action of the excitation force. The important characteristic of vibration caused by such reasons is that the vibration frequency is equal to the rotation frequency or an integer multiple of the rotation frequency. Electromagnetic vibration is mainly caused by the electromagnetic force generated by an unreasonable design of the hydro-generator or poor manufacturing and installation quality. When the hydroelectric generator is running, due to the unbalanced magnetic pull and three-phase imbalance, the thrust tiles are poorly manufactured. The asymmetry of the air gap between the stator and the rotor of the generator and the lax seam of the stator core frame will cause the vibration of the unit and the supporting structure of the unit [28–30]. Vibration caused by mechanical aspects is mainly caused by poor manufacturing and installation quality of turbines and generators, such as axis twists and turns, inclination, poor installation of thrust bearings, and excessive clearance of guide bearings. The vibration caused by mechanical reasons has little to do with the load, and its main vibration frequency is closely related to the rated speed of the unit.

The vibration caused by hydraulic pulsation is the main cause of the vibration of the unit and also the vibration caused by the excitation force acting on the runner [31–33]; its expression is: (1) Water-pressure pulsation caused by water flowing around the blades, which includes two situations caused by poor working conditions and poor blade shape (which is the most important and common cause of excitation), rotation frequency, and blade frequency The pulsating pressure of the three series and the frequency of the guide vane belong to this category; (2) Karman vortex, which is easy to appear only when the shape and size of the blade are inappropriate; (3) draft tube vortex, which often occurs (4) Uneven water inlet to the volute and asymmetric flow path; (5) Others, such as other water-pressure pulsations caused by the above reasons.

2.2. Research on the Characteristics of Vibration Source in Plant Area

2.2.1. Vibration Caused by Vortex Swing and Cavitation in the Draft Tube

(1) Vibration caused by low-frequency vortex swing of draft tube

When the mixed-flow and axial-flow fixed-pitch turbines deviate too much from the design conditions (optimum conditions), sometimes a vortex-swing phenomenon of unsteady flow occurs in the draft tube, forming a vortex motion at the outlet of the runner. It is the main source of low-frequency vibration and noise of the turbine power swing, the rotating part of the unit and the wall of the draft tube, especially in low-load operation, often with relatively large vibration and noise. The fluctuating pressure frequency caused by the draft tube vortex is related to many factors, and is usually calculated by the following empirical formula:

$$f_1 = \frac{n_H}{60}\mu_s \quad (1)$$

where

n_H—unit rated speed, r/min;
μ_s—Turbines with relatively high speed generally take μ_s = 0.03~0.4.

(2) Vibration caused by cavitation

The cavitation of water turbine involves many factors in terms of physics and chemistry, and the incentives it produces are not very clear so far. It is generally believed that the main cause of cavitation is that when the water flow pressure inside the turbine is reduced to the saturated steam pressure, the water vaporizes and a large number of bubbles appear.

During the continuous generation and condensation of bubbles, the high-speed water particles periodically hit the surface of the blade like a sharp knife tip, causing the blade to produce pits, or even be broken down to form a cavity, and at the same time generate vibration. According to experience, the frequency range of pulsating pressure caused by cavitation of turbine runner blades is about 100–300 Hz.

2.2.2. Hydraulic Impact Pulsation of Runner Blades and Guide Vanes

The number of runner blades of a water turbine and the number of water guide vanes have an interactive relationship. During the process of water entering the runner blades from the water guide vanes, once the runner blades and water guide vanes meet, a hydraulic impact will be caused. This kind of impact force acts on the underwater structure through the pier to cause vibration, and the vibration increases with the increase in the load, and its frequency is determined by the number of pulses generated by the interaction between the runner blade and the water guide blade per unit time. Its frequency is calculated as follows:

$$f_2 = \frac{n_H \times Z_1 \times Z_2}{60 \times A} \tag{2}$$

where

Z_1, Z_2—number of runner blades and water guide blades;
A—the greatest common divisor of Z_1 and Z_2;
n_H—unit rated speed, r/min.

2.2.3. Vibration Caused by Uneven Flow Field in Volute

In some working conditions, due to uneven water intake, vortices enter the volute, and these scattered small vortices converge into larger vortex belts and enter the runner to cause vibration, most of which is in the form of medium-frequency vibrations. Sometimes it coincides with the natural vibration frequency of the frame on the generator to generate resonance, which causes the machine pier to vibrate. The vibration frequency caused by the uneven flow field of the volute is the number of runner blades multiplied by the rotational speed frequency, or its multiple (two times, three times, four times), calculated according to the following formula:

$$f_3 = \frac{n_H \times Z_1}{60} \tag{3}$$

In summary, the main vibration sources and frequency characteristics of pumped-storage power plants can be classified into three categories: mechanical vibration, electromagnetic vibration, and hydraulic vibration. The current research on the structural vibration of the underground powerhouse of the pumped-storage power station shows that mechanical vibration and hydraulic vibration are the main vibration sources that cause the vibration of the underground powerhouse structure of the pumped-storage power station.

3. Overview and Finite Element Model of Pumped-storage Power Station

3.1. Overview of Pumped-Storage Power Station

A large-scale pumped-storage power station studied in this paper has an underground powerhouse structure. Four 350 MW reversible mixed-flow pump-turbine units are installed in the power station, with a total installed capacity of 1400 MW. The rated water head is 545 m, the designed annual generating capacity is 2.345 billion kW·h, and the annual pumping power is 3.127 billion kW·h. It is a daily regulation pumped-storage power station. The power station is mainly composed of upper reservoir, water delivery system, underground powerhouse system, ground switch station and lower reservoir, and other buildings. The underground powerhouse adopts the central layout plan, and the water-delivery system adopts the layout of two holes and four machines. The total length of the water-delivery system between the upper and lower reservoir inlets/outlets is about 2764.2 m. Among them, the water-diversion system is about 1245.3 m long, and the tail-water system is 1518.9 m long. The normal storage level of the upper reservoir of

the power station is 867 m, the dead water level is 842 m, and the effective storage capacity is 7.43×10^4 m^3; the normal storage level of the lower reservoir is 306 m, the dead water level is 275 m, and the effective storage capacity is 7.03×10^4 m^3. Dimensions of the main workshop: 112 m × 25 m × 46.85 m (length, width and height); from top to bottom: generator layer, middle layer, water turbine layer, volute layer, etc. The mixed-flow reversible pump-turbine unit adopts the layout of "one machine, one seam", and all structural seams are padded with closed-cell foam boards. The main parameters of the pump-turbine of the pumped-storage power station are shown in Table 1.

Table 1. Main parameters of pump turbine.

Parameter	Unit	Value
Rated head	m	545
Rated output	MW	350
Rated speed	r/min	428
Runaway speed	r/min	620
Number of runner blades	/	11
Number of movable guide vanes	/	20

3.2. Structural Material Properties

The elevation of the volute layer is 195.0 m; the strength grade of the concrete below the volute layer, the concrete surrounding the volute, the windshield of the machine pier and the concrete wall is C30; and the concrete covering the volute and the draft tube concrete have temperature control requirements. The draft tube and volute are made of steel. The geological structure of the project site is simple, the scale of the fault is small, the integrity of the surrounding rock of the underground cavern is good, and the quality of the rock mass is mainly Class II and Class III. The material parameters used in the finite element model are shown in Table 2.

Table 2. Material parameters of finite element model.

Material	Elastic Modulus (MPa)	Poisson's Ratio	Density (kg/m^3)
C30	3.0×10^4	0.2	2500
steel	2.1×10^5	0.3	7800
Type II surrounding rock	1.5×10^4	0.22	2700
Class III surrounding rock	0.8×10^4	0.25	2600

In the numerical simulation of the structural vibration of the underground powerhouse of the project, the following assumptions are made:

(1) The influence of damping is not considered;
(2) Surrounding rock pressure is not considered;
(3) It is considered that the elastic modulus of the surrounding rock is approximately equal to the deformation modulus;
(4) Steel, concrete, and surrounding rock are all regarded as isotropic materials.

3.3. Structural Finite Element Model

The finite element model of the powerhouse structure of the pumped-storage power station takes the main powerhouse structure of the 2# unit section of the powerhouse as the calculation object, and its layout type and structural characteristics are: the upper and downstream side walls of the powerhouse are constrained by the surrounding rock; the lower part of the workshop is mainly a mass concrete structure; and floor slabs, side walls, and structural columns are relatively weak structures of the factory building. In order to make the calculation results more accurate, it is necessary to consider the above-mentioned

types and characteristics, reasonably divide and control the grid of the finite element model, and use a unit form that can reflect the actual component size and structural characteristics of the plant to simulate various structures.

The calculation range is from the boundary along the river to the upstream and downstream side walls connected with the surrounding rock, and the draft tube part is taken to the outlet of the diffusion section (0 + 13.8 m above the powerhouse to 0 + 11.2 m below the powerhouse); the left and right structural joints from the boundary of the horizontal river to the unit section (0 + 11.0 m from the right of the powerhouse to 0 + 37.5 m from the right of the powerhouse); The vertical boundary is from the draft tube bottom plate to the ground elevation of the generator floor (plant vertical ▽183.00 m ~ powerhouse vertical ▽211.15 m). The finite element model includes concrete components such as columns, beams, floor slabs, and side walls of each floor within the scope of the calculation, as well as concrete structures such as machine piers, windshields, volute peripheral support structures, and draft tube peripheral support structures. Also included are runner metal structures such as volutes (ignoring volute seat rings) and draft tubes (including elbows). All concrete structures and larger structural openings are modeled to actual size. Structural holes mainly include demolition holes in machine piers, ventilation holes in wind shields, manholes in volute, manholes in draft pipes, outlet holes for busbars, servo pits in machine piers, holes for stairs and holes for hanging objects, etc. The finite element model of the plant structure is shown in Figure 1.

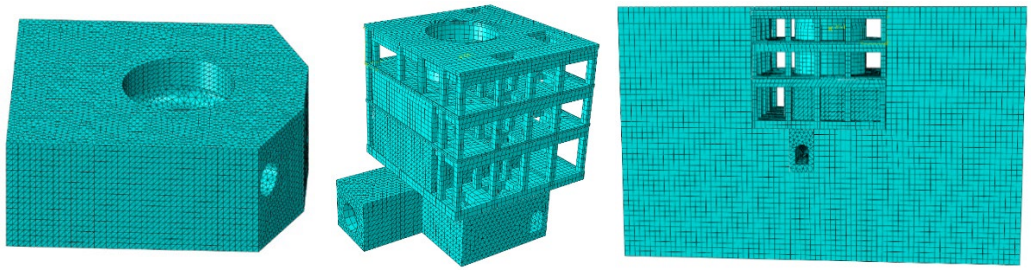

(**a**) (**b**) (**c**)

Figure 1. Finite element model of plant structure: (**a**) Concrete around the volute; (**b**) Plant structure; (**c**) Plant and surrounding rock.

The solid element (C3D8R) is used to simulate large-volume concrete structures such as side walls, floors, machine piers, volutes, draft tubes, and surrounding rocks. The main types of block elements are hexahedron and tetrahedron. The structural system of the underground powerhouse of the pumped-storage power station is very complex, and there are many holes, so it is impossible to use hexahedral elements for better grid division. Therefore, this paper adopts the method of meshing mixed with hexahedral elements and tetrahedral elements. Among them, the hexahedron unit adopts 8-node linear high-precision unit C3D8R, and the tetrahedron unit adopts 10-node quadratic high-precision unit C3D10. The degenerate hexahedron unit is connected between the hexahedron unit and the tetrahedron unit to ensure that the degrees of freedom between the two types of units are fully coordinated. Shell element (S4R), used to simulate the volute and draft-tube steel lining. The surroundings of the finite element model are simulated with infinite element boundary conditions. According to the unit equipment information provided by the unit manufacturer, the operating conditions of the unit mainly considered in the calculation include non-operating conditions, normal operating conditions, runaway conditions, rotor ground faults, out-of-step conditions, etc. Under various working conditions, the loads on the unit act on the stator foundation, the lower frame foundation, and the upper frame foundation.

4. Modal Analysis of Underground Powerhouse Structure

Modal parameters are the inherent properties of building structures, mainly including the natural vibration frequency of the structure, the corresponding structural mode shape, and damping ratio [34–36]. These properties depend on the mass, stiffness distribution, and damping of the structure. These parameters can characterize the dynamic characteristics of the structure itself, and each set of modal parameters corresponds to a specific set of natural frequencies, mode shapes, and damping ratios. Through modal analysis, we can understand the vibration characteristics of each order of the structure in the vulnerable frequency range, so that we can predict the actual vibration characteristics of the structure in this frequency range under the action of various external or internal vibration sources. In order to study the influence of the dynamic elastic modulus of materials on the vibration response of the plant structure, six different calculation schemes are proposed, and the specific calculation schemes are shown in Table 3. Figure 2 shows the main mode diagrams of the first two orders of free vibration for calculation conditions one to six. In the actual engineering project of pumped-storage power station, the geology and bottom layer will be more complicated. When carrying out structural design, it can only be analyzed based on some representative hole geology obtained from a geological survey. However, in order to avoid the actual geological differences from affecting the dynamic characteristics of the hydro-power plant, and to leave a certain safety margin, it is necessary to conduct a sensitivity analysis of the dynamic-elastic model characteristics of the rock formations around the underground power plant of the hydropower station.

Table 3. Calculation conditions.

Conditions	1	2	3	4	5	6
Dynamic modulus of elasticity	1.0 *E*	1.1 *E*	1.2 *E*	1.3 *E*	1.4 *E*	1.5 *E*

Note: *E* in the table represents the static elastic modulus of the material.

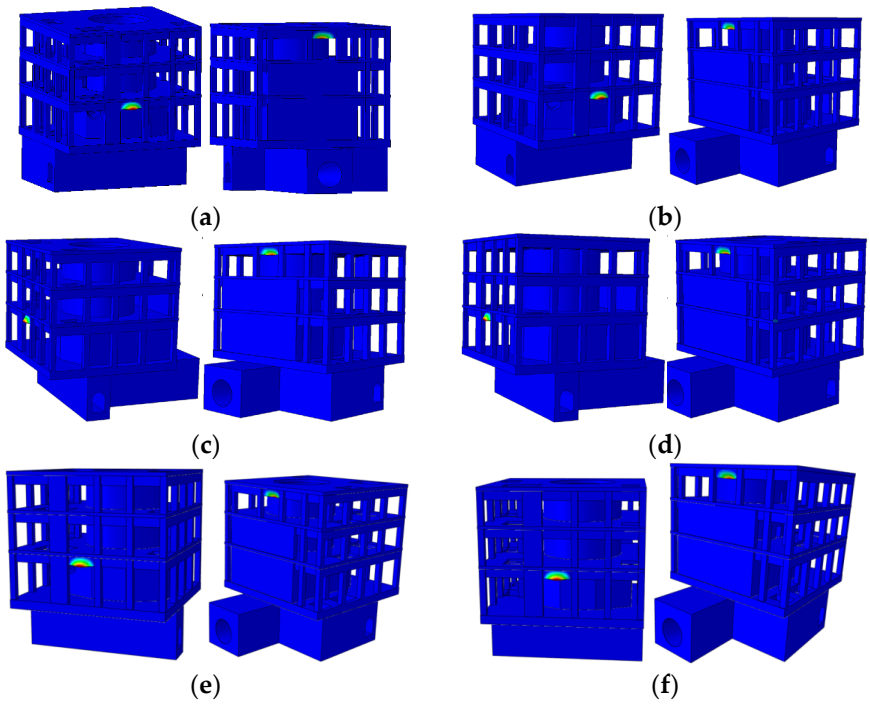

Figure 2. The first two vibration modes of each working condition: (**a**) Condition 1; (**b**) Condition 2; (**c**) Condition 3; (**d**) Condition 4; (**e**) Condition 5; (**f**) Condition 6.

Based on the calculation results, statistics are made on the natural vibration frequency of the plant structure under each working condition, and the statistical results are shown

in Table 4. It can be seen from Table 4 that the structural natural vibration frequency calculated by the dynamic elastic modulus is higher than that calculated by the static elastic modulus, and the first-order frequencies of the free vibration of the structure in working conditions 1–2 are 15.07 Hz, 18.25 Hz, 19.06 Hz, 19.84 Hz, 20.58 Hz, 21.31 Hz. With the increase in the dynamic elastic modulus of the structure, the overall stiffness of the plant structure increases, so the natural vibration frequency of the structure also increases. The fundamental frequency of the overall structure of the plant increases linearly with the increase in the dynamic elastic modulus of the structure, and the fundamental frequency of working condition six is about 29% higher than that of working condition one. It shows that the natural frequency of the structure is directly related to the elastic modulus of the material. The mode shapes of each order under the six working conditions basically remain unchanged, indicating that the elastic modulus has little influence on the mode shape of the factory building structure, but the natural vibration frequency increases linearly with the increase in the dynamic elastic modulus.

Table 4. Natural frequency statistics of plant structure.

Step	Frequency/Hz						$\frac{(6)-(1)}{(6)} \times \%$
	Condition 1	Condition 2	Condition 3	Condition 4	Condition 5	Condition 6	
1	15.07	18.25	19.06	19.84	20.58	21.31	29.287%
2	15.23	18.45	19.27	20.05	20.81	21.54	29.288%
3	16.20	19.62	20.49	21.32	22.13	22.91	29.291%
4	16.23	19.65	20.52	21.36	22.17	22.95	29.291%
5	16.62	20.12	21.02	21.88	22.70	23.50	29.291%
6	17.21	20.84	21.77	22.66	23.51	24.34	29.290%
7	17.23	20.87	21.80	22.69	23.54	24.37	29.287%
8	17.67	21.40	22.36	23.27	24.15	24.99	29.288%
9	17.84	21.60	22.56	23.48	24.37	25.23	29.288%
10	18.06	21.87	22.84	23.78	24.68	25.54	29.290%

According to the excitation frequency of various vibration sources in the plant area of the pumped-storage power station, combined with the natural vibration frequency of the underground powerhouse structure, one must refer to the regulations on resonance verification in the "Code for Design of Hydropower Station Buildings" (NB/T35011-2016) [37]: "The ratio of the difference between the natural vibration frequency of the pier and the forced vibration frequency to the natural frequency should be greater than 20%, or the ratio between the difference between the forced vibration frequency and the natural frequency and the forced vibration frequency of the pier should be greater than 20% to prevent resonance". The resonance check of the powerhouse structure of the pumped-storage power station is carried out. The comparison between the main excitation frequency and the natural frequency of the underground powerhouse structure is now listed in Table 5, and the possibility of resonance can be checked from the results.

It can be seen from the results in Table 5 that the natural vibration frequency of the unit is 7.1 Hz at the rated speed and 10.3 Hz at the runaway speed. There is a large difference between the fundamental frequency of the plant structure and the rotation frequency of the unit, which will not cause resonance; the low-frequency and high-frequency excitation and the natural vibration frequency of the plant structure are greatly staggered, and there is no possibility of resonance. The main possible resonance areas are the double frequency (14.2 Hz) and triple frequency (21.3 Hz) of the unit's rotation frequency. It can be considered that the factory building should be closely integrated with the surrounding rock as much as possible, so as to improve the overall rigidity of the factory building structure and improve the anti-vibration performance.

Table 5. Resonance check of powerhouses.

f_j		f_z							
		1	**2**	**3**	**4**	**5**	**6**	**7**	**8**
		0.2~2.9	**6.4~8.6**	**7.1**	**10.5**	**14.2**	**21.3**	**78.6**	**157.2**
No.	**Value**	$\lvert (f_j - f_z)/f_j \rvert \times 100\%$							
1	15.07					5.8			
2	15.23					6.8			
3	16.20					12.3			
4	16.23					12.5			
5	16.62					14.6			
6	17.21					17.5			
7	17.23					17.6			
8	17.67					19.6			
9	17.84						19.4		
10	18.06						17.9		
11	18.37						15.9		
12	19.32						10.2		
13	22.40						4.9		
14	22.67						6.0		
15	23.18						8.1		
16	23.49						9.2		
17	23.61						9.8		
18	23.69						10.1		
19	24.00						11.3		
20	24.23						12.1		

Note: f_j—natural frequency; f_z—excitation frequency.

5. Analysis of Steady-State Response Characteristics of Powerhouse Structure

5.1. Steady-State Process Calculation Principle

The mass matrix and stiffness matrix of the structure are calculated by the finite element program, and the concrete elastic modulus is valued according to the dynamic elastic modulus. When calculating the structural mass matrix, only the self-weight of the underground powerhouse structure and mechanical equipment are considered, and the self-weight of the water body is not included. The mass is calculated according to the standard value of the load, without considering the sub-item factor of the load, the structural importance factor and the design condition factor, etc. The calculation method of mass matrix and stiffness matrix is the same as that of structure-free vibration calculation [38–40]. After decoupling with mode shape coordinates, independent equations can be obtained:

$$\ddot{q}_i + 2\varsigma_i\omega_i\dot{q}_i + \omega_i^2 q = f_i(t) \tag{4}$$

where m is the number of mode shapes selected in the calculation, ζ_i is the damping ratio, and $f_i(t)$ is the i-mode shape function.

When solving the steady-state response, the dynamic load can be expressed as:

$$\{P(t)\} = \{P_r\}\cos\omega t + \{P_i\}\sin\omega t \tag{5}$$

where $\{P_t\}$ and $\{P_i\}$ are the real and imaginary parts of the load amplitude, respectively. ω is the circular frequency of the excitation force.

$$f_i(t)\} = \{\phi_i\}^T\{P(t)\} = f_{ri}\cos\omega t + f_{ii}\sin\omega t \tag{6}$$

The m independent vibration equations become:

$$\ddot{q}_i + 2\varsigma_i\omega_i\dot{q} + \omega_i^2 q = f_{ri}\cos\omega t + f_{ii}\sin\omega t \tag{7}$$

Consider only steady-state solutions of the equation:

$$q_i(t) = A_i \cos(\omega t - \theta_i) + B_i \sin(\omega t - \theta_i) \tag{8}$$

After substituting into the vibration equation, we can get:

$$A_i = \frac{f_{ri}}{\omega_i^2}\beta_i, B_i = \frac{f_{ii}}{\omega_i^2}\beta_i, tg\theta_i = \frac{\alpha\xi_i\omega/\omega_i}{1-\omega^2/\omega_i^2}, \beta_i = \frac{1}{\sqrt{(1-\frac{\omega^2}{\omega_i})^2 + (\alpha\xi_i\frac{\omega}{\omega_i})^2}} \tag{9}$$

where β_i is the i-order dynamic amplification factor, and θ_i is the phase difference. After calculating $q_i(t)$, the displacement response can be calculated:

$$\{u\} = [\Phi]\{q\} = [\{\phi_1\}, \{\phi_2\}, \cdots \{\phi_m\}]\begin{Bmatrix} q_1 \\ q_2 \\ \vdots \\ q_m \end{Bmatrix} \tag{10}$$

Each node displacement can be written as:

$$u_k(t) = C_k \cos(\omega t - \theta_k) + D_k \sin(\omega t - \theta_k) \tag{11}$$

Among them, C_k and D_k are constants, respectively representing the displacement amplitude of the real part and the displacement amplitude of the imaginary part.

The node acceleration is:

$$\ddot{u}_k(t) = -\omega^2[C_k \cos(\omega t - \theta_k) + D_k \sin\cos(\omega t - \theta_k)] = -\omega^2 u_k(t) = -4\pi^2 f^2 u_k(t) \tag{12}$$

For normal operating conditions, rotor ground fault conditions and out-of-step conditions, the relationship between displacement and acceleration at this time is:

$$\ddot{u}_k(t) = -4\pi^2 8.333^2 u_k(t) = -2741.3 u_k(t) \tag{13}$$

For the runaway operating condition, the relationship between displacement and acceleration at this time is:

$$\ddot{u}_k(t) = -4\pi^2 12.083^2 u_k(t) = -5763.8 u_k(t) \tag{14}$$

After calculating the structural node displacement, the node acceleration can be calculated according to the above formula.

5.2. Steady-State Calculation Conditions and Loads

For the steady-state process of power station operation, the location of the maximum vibration displacement of the underground powerhouse structure of the pumped-storage power station can be obtained by calculating the vibration amplitude of each calculation point of the four different boundary condition models. Following this, one must carry out and check whether the maximum vertical displacement and maximum horizontal displacement of the power station meet the design requirements during steady-state operation, and provide a reference for the layout of measuring points for on-site vibration testing.

In order to study the different connection forms between the upstream and downstream side walls and the surrounding rock, and the influence of different lithology surrounding rock on the dynamic response of the plant structure, four finite element models were established. Among them, model one is the calculation model of underground powerhouse structure without considering the effect of surrounding rock, models two to four are calculation models of underground powerhouse structure considering the effect of

surrounding rock, and the joints of the unit components are free boundaries. The specific processing methods of the boundary conditions of the four models are as follows:

(1) Model 1: Only the powerhouse structure model is established, without considering the effect of surrounding rock, fixed constraints are taken on the upstream and downstream surfaces and bottom, and normal constraints are taken on the downstream surface of the draft tube.
(2) Model 2: Establish the plant structure and surrounding rock model, and establish binding constraints for the boundary nodes of the plant side wall and the surrounding rock to deform together. The deformation modulus of the surrounding rock is selected according to the type II surrounding rock, and the deformation modulus is 4.0 × 104 Mpa, and the Poisson's ratio is 0.23. The upstream and downstream surfaces and sides of the surrounding rock are constrained by the normal direction, and the bottom is fixed.
(3) Model 3: Establish the plant structure and surrounding rock model, and establish binding constraints for the boundary nodes of the plant side walls to deform together. The deformation modulus of the surrounding rock is selected according to the type III surrounding rock, and the deformation modulus is 3.0 × 104 MPa, and Poisson's ratio is 0.28. The upstream and downstream surfaces and sides of the surrounding rock are constrained by the normal direction, and the bottom is fixed.
(4) Model 4: Establish the plant structure and surrounding rock model, and establish binding constraints for the boundary nodes of the plant side walls to deform together. The rock deformation modulus is selected according to Class II surrounding rock, and the deformation modulus is 4.0 × 104 MPa, and Poisson's ratio is 0.23. The upstream and downstream surfaces, sides and bottom of the surrounding rock are fully fixed.

When calculating various operating conditions in the dynamic response steady-state process, only the dynamic load of the unit is considered, and the influence of other loads is not considered. There are mainly three types of dynamic loads generated during unit operation:

(1) Vertical dynamic load: including generator rotor, turbine runner, axial water thrust, etc.;
(2) Tangential dynamic load: normal torque, two-phase short-circuit torque and out-of-step torque;
(3) Radial dynamic load: When the generator is running, it is caused by magnetic and mechanical imbalance, a short circuit of half of the magnetic poles, and temperature change.

The above dynamic loads are all assumed to be simple harmonic loads, which act on the upper frame foundation, stator foundation, and lower frame foundation of the machine pier. The steady-state dynamic response of the structure is calculated according to the harmonic response method, and the standard value of the dynamic load of the unit is applied to each foundation plate corresponding to the machine pier after deducting the self-weight of the equipment. Statistical table of frequency and amplitude standard value of dynamic load on foundation plate are shown in Table 6.

Table 6. Statistical table of frequency and amplitude standard value of dynamic load on foundation plate.

Conditions	Frequency (Hz)	Standard Value of Load Amplitude (kN)						
		Stator Foundation			Stator Foundation		Stator Foundation	
		F1 Vertical	F2 Radial	F3 Tangential	F4 Radial	F5 Tangential	F6 Radial	F7 Tangential
Normal operation	7.14	241.4	120.4	542	298	200	10	2

5.3. Calculation Result Analysis of Steady State Process

The steady-state process calculation is mainly to calculate the vibration displacement amplitude of the structural floor of the underground powerhouse, understand the vibration displacement characteristics of the structure, and find the location where the maximum vibration displacement occurs. In order to describe the calculation results, a total of 43 calculation points are selected according to different representative parts of the floor, and the vibration displacement values of these 43 points are used to reflect the vibration displacement characteristics of the structure, and the point where the maximum vibration displacement occurs is determined by comparison. The 43 points are distributed on the floor of the generator floor, the floor of the middle floor, the center of the stator foundation plate above the demolition hole in the machine pier, and the floor of the turbine floor. The positions of the points are shown in Figure 3.

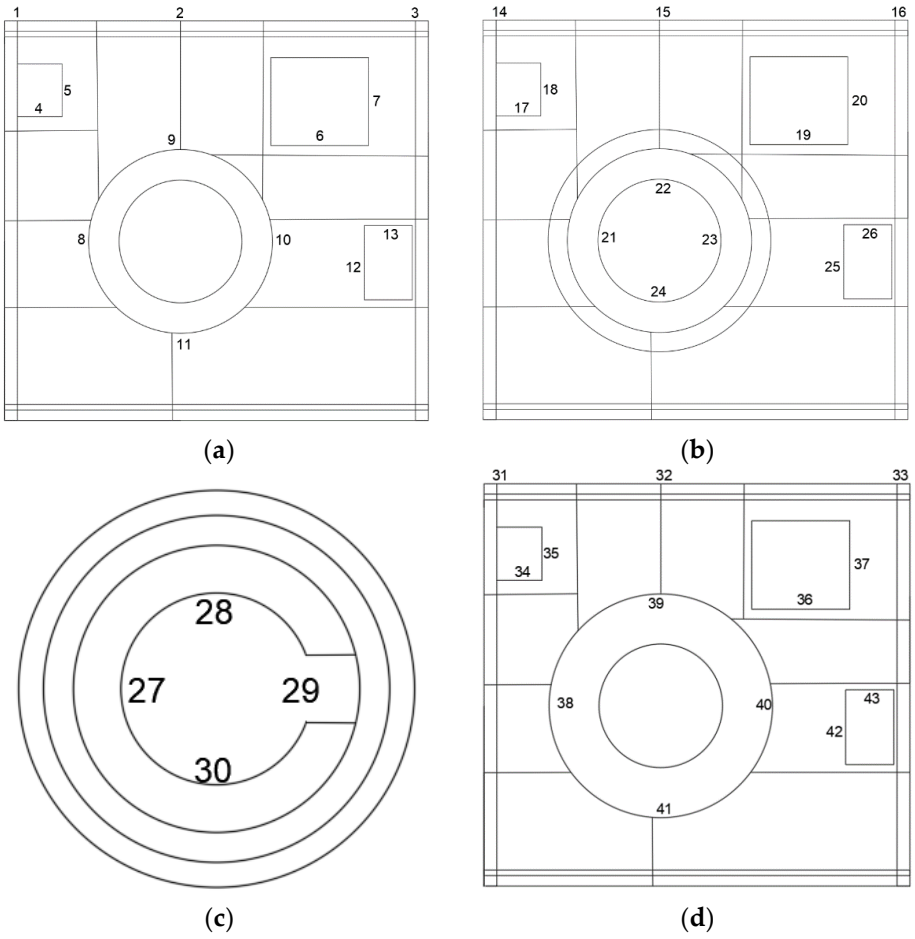

Figure 3. Location layout of displacement calculation points: (**a**) Calculation point of floor displacement on generator floor; (**b**) Calculation point of floor displacement on middle floor; (**c**) Displacement calculation point of stator foundation; (**d**) Calculation point of turbine floor displacement. The vibration displacement amplitudes in all directions of the plant structure during the steady state process of the unit are shown in Figures 4–6. It can be seen from Figures 4–6 that the vertical vibration displacement is larger than the horizontal vibration displacement. Among them, the point numbers with large vertical vibration displacement mainly include 9, 10 (top of windshield), 21, 22 (top of machine pier), 29, 30 (stator foundation), 40, 41 (lower frame foundation), etc. The measuring points in this analysis are layered from left to right, and the measuring points are set separately for key parts. It is precisely because of the difference in the positions of the displacement measuring points that the zigzag fluctuations of the displacement curves in Figures 4–6 are caused.

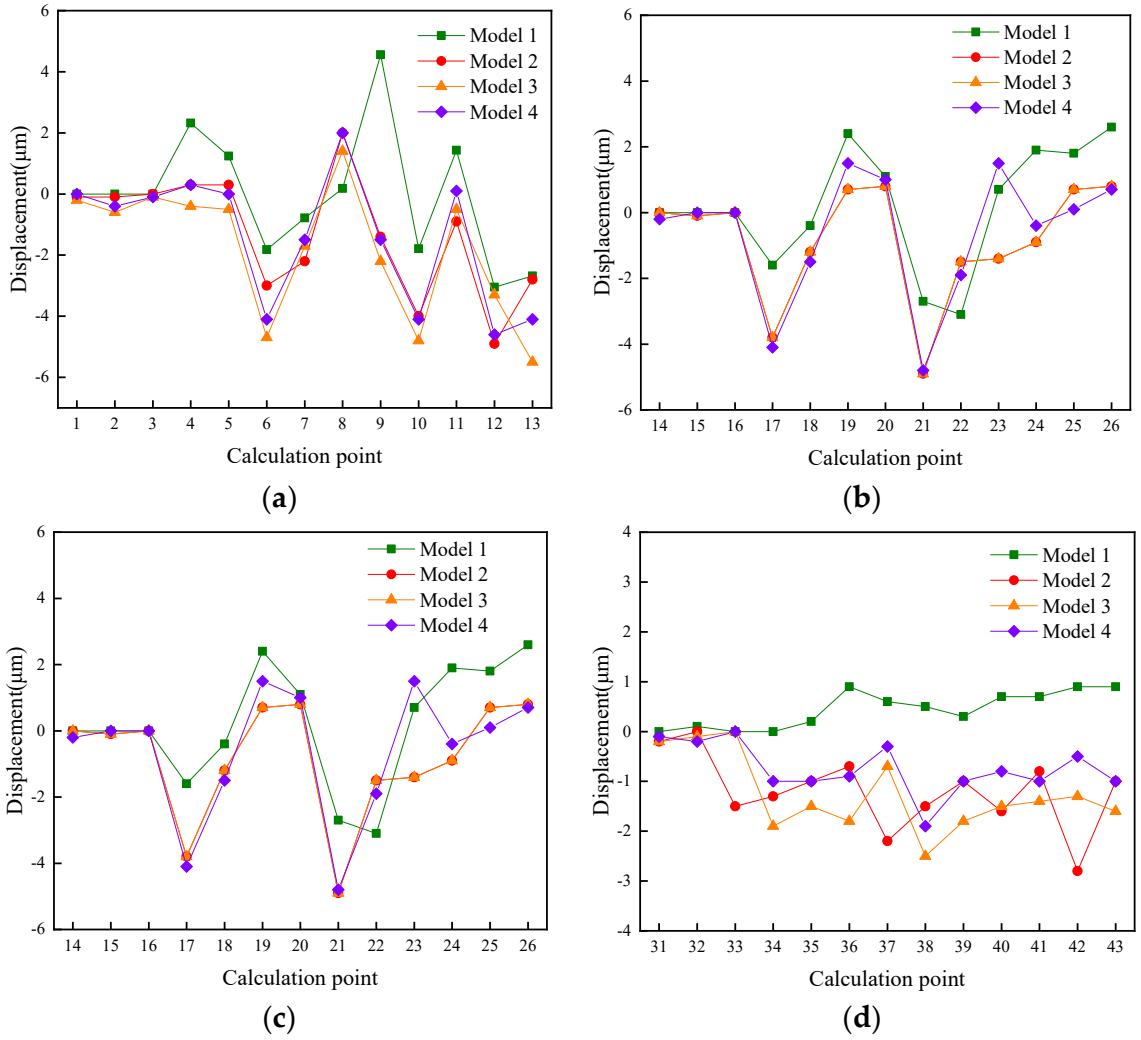

Figure 4. Amplitude of horizontal vibration displacement: (**a**) generator layer; (**b**) middle layer; (**c**) stator foundation plate; (**d**) turbine layer.

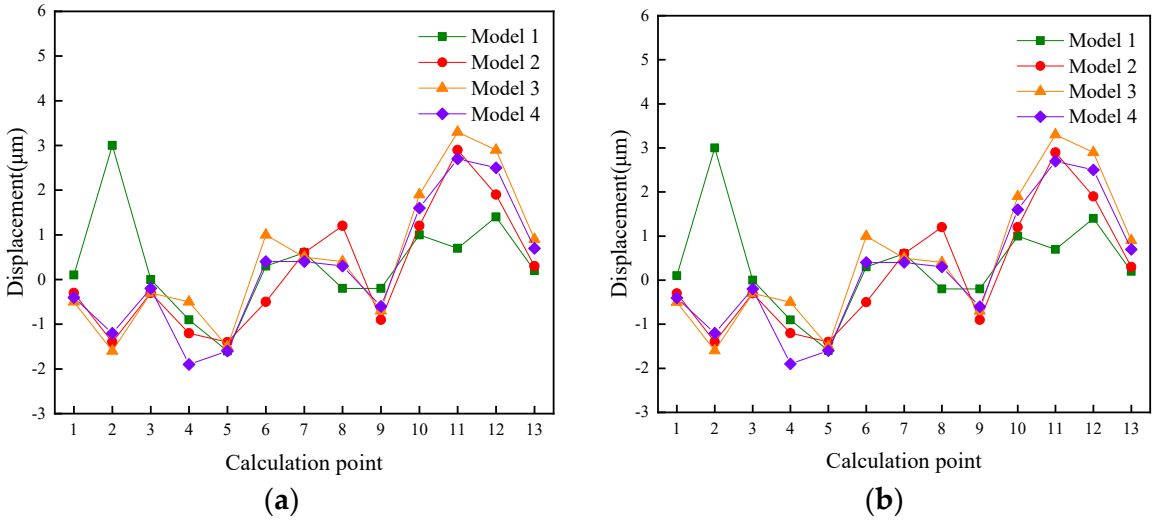

Figure 5. *Cont*.

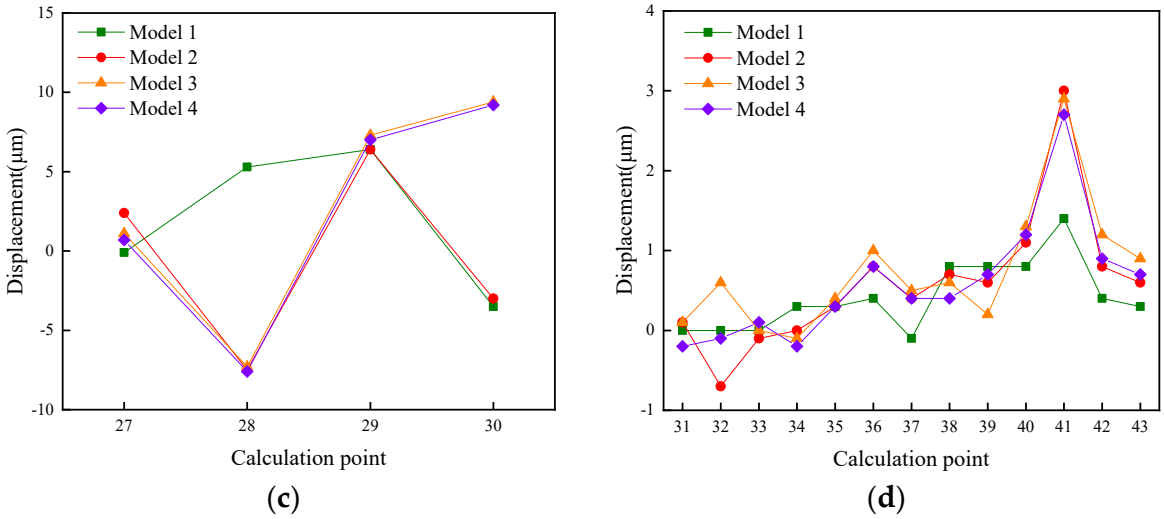

Figure 5. Amplitude of vibration displacement along the river: (**a**) generator layer; (**b**) middle layer; (**c**) stator foundation plate; (**d**) turbine layer.

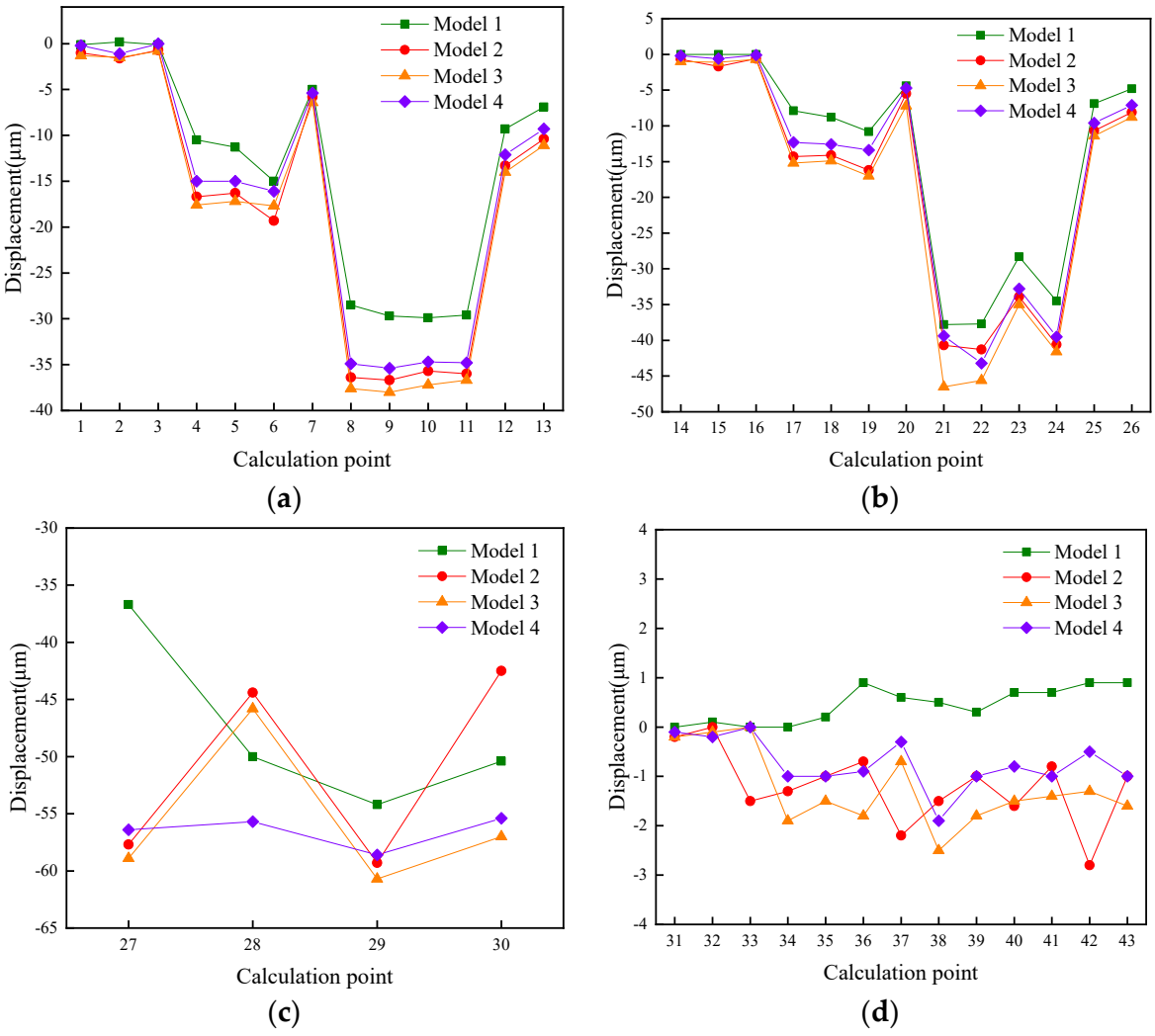

Figure 6. Vertical vibration displacement amplitude: (**a**) generator layer; (**b**) middle layer; (**c**) stator foundation plate; (**d**) turbine layer.

Table 7 shows the statistics of the locations with larger vibration displacements in the steady-state process. When arranging measuring points for on-site inspection, the vibration displacement measuring points should be arranged around these point numbers. It can be seen from Table 7 that the large value of the vibration displacement in the steady-state process mainly occurs at the top of the windshield on the generator floor, the ball valve hanging hole on the generator floor, the rectangular long hole upstream of the generator floor, the outer side of the opening of the stairwell on the middle floor, the top of the machine pier on the middle floor, the lifting hole of the ball valve on the middle floor, and the stator foundation plate above the demolition hole in the machine pier. During on-site inspection, vibration displacement measurement points should be arranged near the displacement calculation points of these parts, and the vibration-displacement measurement points should be arranged at openings such as lifting holes and stairwells.

Table 7. Point number and location with large vibration displacement in steady state process.

Conditions	Point Number	Location
Generator layer	4, 5	Rectangular lifting hole upstream of the floor
	6, 7	Lifting hole of the ball valve on the floor plate of the generator
	8, 9, 10, 11	Windshield top
	12, 13	Floor stairwell
Middle layer	19, 20	Middle layer ball valve hanging hole
	21, 22	Machine pier top
	27, 28, 29, 30	Stator foundation

The maximum vibration-displacement amplitude of each model and the corresponding point number and location are shown in Table 8. It can be seen from Table 8 that the maximum vibration displacement mainly occurs at points 27, 28, 29, and 30. The horizontal vibration displacement of each model in the steady-state process is small. The maximum vibration displacement of the factory building in the horizontal direction is 7.6 μm (Model 1), the maximum vibration displacement of the factory building in the river direction is 9.4 μm (Model 3), the vertical displacement of the factory building is relatively large, and the maximum vertical vibration displacement is −60.7 μm (Model 3).

Table 8. The maximum vibration-displacement amplitude of each model (μm).

Condition	Model	X (Horizontal)		Y (Forward)		Z (Vertical)	
		No.	Displacement	No.	Displacement	No.	Displacement
Steady state process	1	27	7.6	29	6.4	29	−54.2
	2	29	−5.8	28	−7.5	29	−59.3
	3	29	−6.3	30	9.4	29	−60.7
	4	29	−5.6	30	9.2	29	−58.6

According to the provisions of Article 6.3.8 of the "Design Code for Powerhouses of Hydropower Stations" (NB/T35011-2016) [37], the amplitude of the forced vibration of the machine pier should meet the following criteria: the vertical amplitude is not greater than 0.15 mm (150 μm), and the sum of the horizontal transverse and torsional amplitudes is not greater than 0.2 mm (200 μm). Considering that the structural importance coefficient is taken as 1.1, the maximum value of the vertical vibration displacement of the plant during the steady-state process of this project is 1.1 × 60.7 μm = 66.8 μm < 1500 μm, which meets the design requirements. In the steady state process, the maximum horizontal vibration displacement of the plant is $1.1 \times \sqrt{9.4^2 + 7.6^2} = 12.1$ μm ≤ 200 μm, which meets the design requirements. Therefore, the vibration displacement of the underground powerhouse structure in the steady-state process meets the design requirements.

6. Conclusions

This paper takes a large-scale pumped-storage power station as the research object, and conducts numerical simulation research on the underground powerhouse structure of the project, including modal analysis and dynamic response analysis of the steady-state process of the unit under different boundary conditions. The calculation results of the project show that:

(1) The fundamental frequency of the plant structure and the excitation frequency of the main vibration source are greatly staggered, and resonance will not be induced. Moreover, the mode shape of each order of the plant structure does not change much, mainly manifested as the vibration of the beam-system structure. This is because the stiffness of the beam-system components is much smaller than that of the wind cover, machine pier, and mass concrete around the volute.

(2) According to the calculation results of the dynamic response of the plant in the steady-state process of the unit, the maximum vibration displacement of each calculation point of the plant structure meets the design requirements. The calculation results also reflect the distribution law of the larger vibration displacement positions of the plant structure. It can provide a theoretical reference for the layout of measuring points for plant safety monitoring, and has guiding significance for the anti-vibration and vibration-reduction design of underground plant structures of pumped-storage power stations.

(3) Considering the influence of different connection forms between the upstream and downstream side walls and surrounding rocks on the dynamic response of the factory building structure, four kinds of factory-building-structure models were established. The calculation results of this project show that the maximum displacement of the factory building structure in all directions meets the design requirements. In addition, the distribution law of the large vibration-displacement position of the plant structure is revealed, which can provide a theoretical reference for the arrangement of measuring points for plant safety monitoring.

Author Contributions: Methodology, L.Z., H.W. and J.L.; numerical analysis, Y.G. and X.Y.; writing—original draft preparation, Y.G. and X.Y. All authors have read and agreed to the published version of the manuscript.

Funding: The authors would like to acknowledge the support from the Joint Independent Innovation Fund of Qinghai Minzu University of China and Tianjin University of China (Grant Nos. 2022TQ01 and 2022XSU-0011).

Conflicts of Interest: The authors declare no conflict of interest.

References

1. Lian, J.; Zhang, Y.; Ma, C.; Yang, Y.; Chaima, E. A review on recent sizing methodologies of hybrid renewable energy systems. *Energy Convers. Manag.* **2019**, *199*, 112027. [CrossRef]
2. Mahlia, T.M.I.; Saktisandan, T.J.; Jannifar, A.; Hasan, M.H.; Matseelar, H.S.C. A review of available methods and development on energy storage; technology update. *Renew. Sustain. Energy Rev.* **2014**, *33*, 532–545. [CrossRef]
3. Hemmati, R.; Saboori, H. Emergence of hybrid energy storage systems in renewable energy and transport applications—A review. *Renew. Sustain. Energy Rev.* **2016**, *65*, 11–23. [CrossRef]
4. Koohi-Fayegh, S.; Rosen, M.A. A review of energy storage types, applications and recent developments. *J. Energy Storage* **2020**, *27*, 101047. [CrossRef]
5. Koohi-Kamali, S.; Tyagi, V.V.; Rahim, N.A.; Panwar, N.L.; Mokhlis, H. Emergence of energy storage technologies as the solution for reliable operation of smart power systems: A review. *Renew. Sustain. Energy Rev.* **2013**, *25*, 135–165. [CrossRef]
6. Zhang, H.; Baeyens, J.; Caceres, G.; Degreve, J.; Lv, Y. Thermal energy storage: Recent developments and practical aspects. *Prog. Energy Combust. Sci.* **2016**, *53*, 1–40. [CrossRef]
7. Zhang, H.; Huys, K.; Baeyens, J.; Degreve, J.; Kong, W.; Lv, Y. Thermochemical Energy Storage for Power Generation on Demand. *Energy Technol.* **2016**, *4*, 341–352. [CrossRef]
8. Fernandes, D.; Pitie, F.; Caceres, G.; Baeyens, J. Thermal energy storage: "How previous findings determine current research priorities". *Energy* **2012**, *39*, 246–257. [CrossRef]

9. Suberu, M.Y.; Mustafa, M.W.; Bashir, N. Energy storage systems for renewable energy power sector integration and mitigation of intermittency. *Renew. Sustain. Energy Rev.* **2014**, *35*, 499–514. [CrossRef]
10. Groppi, D.; Pfeifer, A.; Garcia, D.A.; Krajac, G.; Duic, N. A review on energy storage and demand side management solutions in smart energy islands. *Renew. Sustain. Energy Rev.* **2021**, *135*, 110183. [CrossRef]
11. Wang, X.; Yu, J. The operation strategy and its benefit assessment of the distributed pumped storage system. *Power Syst. Prot. Control.* **2012**, *40*, 129–137+142.
12. Rehman, S.; Al-Hadhrami, L.M.; Alam, M.M. Pumped hydro energy storage system: A technological review. *Renew. Sustain. Energy Rev.* **2015**, *44*, 586–598. [CrossRef]
13. Mansoor, S.P.; Munoz-Hernandez, G.A. Development of gain scheduling scheme for pumped storage plant. In Proceedings of the 9th IASTED International Conference on Intelligent Systems and Control, Honolulu, HI, USA, 14–16 August 2006; p. 13.
14. Ramos, H.M.; Dadfar, A.; Besharat, M.; Adeyeye, K. Inline Pumped Storage Hydropower towards Smart and Flexible Energy Recovery in Water Networks. *Water* **2020**, *12*, 2224. [CrossRef]
15. Wang, H.; Mao, L.; Lian, J. Structural vibration prediction for a hydropower house based on RVM method. *J. Vib. Shock.* **2015**, *34*, 23–27.
16. Fitzgerald, N.; Arantegui, R.L.; McKeogh, E.; Leahy, P. A GIS-based model to calculate the potential for transforming conventional hydropower schemes and non-hydro reservoirs to pumped hydropower schemes. *Energy* **2012**, *41*, 483–490. [CrossRef]
17. Valavi, M.; Nysveen, A. Variable-Speed Operation of Hydropower Plants. *IEEE Ind. Appl. Mag.* **2018**, *24*, 18–27. [CrossRef]
18. Kuiwei, Z.H.U. Summarization of safety monitoring on underground works of Baishan Pumped Storage Hydropower Station. *Water Resour. Hydropower Eng.* **2008**, *39*, 59–62.
19. Li, Y.; Zhu, X. Measurement and control of vibration from blasting construction of rock-bolted crane beam in underground powerhouse of Hongping Pumped Storage Hydropower Station. *Water Resour. Hydropower Eng.* **2015**, *46*, 77–79+83.
20. Chen, J.; Yang, T. Water filling and discharging test for tailrace system of Xianyou Pumped Storage Hydropower Station. *Water Resour. Hydropower Eng.* **2015**, *46*, 41–45.
21. Dechang, X.U.; Jigong, L.I.; Genyi, Z.U. Reservoir operation of Baishan Pumped Storage Hydropower Station during construction period. *Water Resour. Hydropower Eng.* **2008**, *39*, 78–80.
22. Kiene, S.; Linkevics, O. Simplified model for evaluation of hydropower plant conversion into pumped storage hydropower plant. *Latv. J. Phys. Tech. Sci.* **2021**, *58*, 108–120. [CrossRef]
23. Xiaojun, H.; Bingfang, W.; Min, A.I. Analysis on monitoring of underground powerhouse and water conduit system during water filling and storing process at Langyashan Pumped Storage Hydropower Station. *Water Resour. Hydropower Eng.* **2008**, *39*, 79–82.
24. Jia, D.; Cheng, L. Research on Development of Pumped-Storage Hydropower in Northwest of China. *Electr. Power* **2012**, *45*, 5–7.
25. Xiaoxia, C.; Lin, F.; Runbao, Y. Study on vibration of trash-rack for Baishan Pumped Storage Hydropower Station. *Water Resour. Hydropower Eng.* **2008**, *39*, 63–66.
26. Jing, Y.; Kui, W.U. Analysis of the factors that affect the arrangement of powerhouse of pumped storage power station. *J. Hydroelectr. Eng.* **2009**, *28*, 114+157–160.
27. Zhang, H.; Chen, D.; Xu, B.; Patelli, E.; Tolo, S. Dynamic analysis of a pumped-storage hydropower plant with random power load. *Mech. Syst. Signal Process.* **2018**, *100*, 524–533. [CrossRef]
28. Xueyuan, Z.; Enbo, Z. Analysis on dynamic water closing test of butterfly valve for hydro-power unit in Baishan Pumped Storage Hydropower Station. *Water Resour. Hydropower Eng.* **2008**, *39*, 39–41.
29. Zhao, X.; Gao, L. Study on availability of weathered-rock materials for construction of dam for Wendeng Pumped Storage Hydropower Station. *Water Resour. Hydropower Eng.* **2014**, *45*, 73–76.
30. Zhou, H. Method for water filling and discharging test on water delivery system of Pushihe Pumped Storage Hydropower Station. *Water Resour. Hydropower Eng.* **2015**, *46*, 86–87+90.
31. Jijian, L.; Liang, Q.I.N.; Huijing, T.; Wei, Z.; Chenglian, H.E. Vibration analysis of hydropower-house during start-up process. *J. Hydroelectr. Eng.* **2006**, *25*, 1–5+15.
32. Lian, J.; Hu, Z.; Qin, L.; Wang, R. Study on dynamic characteristics of unit supporting structure of underground power-house of large hydropower station. *J. Hydroelectr. Eng.* **2004**, *23*, 49–54.
33. Lian, J.; Qin, L.; Wang, R.; Hu, Z.; Wang, H. Study on the dynamic characteristics of the power house structure of two-row placed units. *J. Hydroelectr. Eng.* **2004**, *23*, 55–60.
34. Cheng, S.; Li, S.; Si, Z.; Bi, C.; Yang, Y.; Chen, Y. Relational grade analysis for influencing factors and the natural vibration frequency of hydropower house. *S. N. Water Transf. Water Sci. Technol.* **2017**, *15*, 190–196+203.
35. Geng, D.; Song, Z.; Su, C. Review on the Impact of Hydraulic Vibration on Hydropower Unit and Hydropower House and Vibration Control. *J. Yangtze River Sci. Res. Inst.* **2016**, *33*, 135–139.
36. Peng, G.; Qin, L.; Wang, Z.; Tian, H.; Luo, Y.; ASME. Structure Vibration of Hydropower House Induced by Francis Turbine Based on CFD. In Proceedings of the ASME Fluids Engineering Division Summer Conference, Jacksonville, FL, USA, 10–14 August 2008; pp. 1173–1178.
37. *NB/T35011-2016*; People's Republic of China Energy Industry Standards: Design Code for Powerhouses of Hydropower Stations. Chinese Standard: Beijing, China, 5 December 2016.
38. Yunhe, L.I.U.; Xingjun, S.; Shouyi, L.I. Study on dynamic characteristics of overflow hydropower house structure. *J. Hydroelectr. Eng.* **2007**, *26*, 39–43.

39. Zhang, C.; Ma, Z.; Zhou, S.; Zhang, Y. Analysis of fluid-solid interaction vibration characteristics of large-scale hydropower house. *J. Hydroelectr. Eng.* **2012**, *31*, 192–197.
40. Song, Z.; Zhao, E. Analysis on endogenous vibrations of hydropower house on soft foundation. *J. Hydroelectr. Eng.* **2014**, *33*, 181–186.